REMOTE SENSING OF SHALLOW WATER BREAKING WAVES

Reprinted from Proceedings of Waves 2001
San Francisco, CA – Sept, 2001

Merrick C. Haller [1] and David R. Lyzenga [2]

Abstract: This paper compares simultaneous microwave radar and video camera signals from shallow water breaking waves. The results show that the radar cross section (RCS) is well correlated with the size of the turbulent breaking region estimated from the video camera. This indicates that microwave radar is a good breaking wave detector and can be used for the measurement of the spatial and temporal variations of wave breaking. In addition, microwave radar offers the advantage of not being sensitive to relict foam generated in the breaking process. Finally, the RCS per unit area of the turbulent breaking region appears to be well approximated by a constant value of -2 dB ($\pm$ 0.5 dB).

INTRODUCTION

The measurement of the location and frequency of wave breaking events in shallow water is of significant interest because these events are the dominant forcing mechanism in the nearshore region. The breaking process transfers most of the energy and momentum associated with the organized wave motion into longshore currents, low frequency gravity wave motions, and turbulence. Additionally, the movement of sediment in the surf zone is closely related to these energy transfer processes and the beach topography is often encoded in the spatial variability of wave breaking (Lippmann and Holman 1989).

Quantitative field measurements of wave breaking events are generally difficult, especially with in-situ sensors. A wide range of measurement types have been tested including: sea surface elevation, void fraction (Gemmrich and Farmer 1999), underwater sound (Ding and Farmer 1994), infrared surface properties (Jessup et al. 1997), and microwave backscatter. However, it is clear that remote sensing techniques are the only feasible method for obtaining measurements of wave breaking with large spatial coverage. To date, visual recording of break-

[1]Ocean Engineering Program, Dept. of Civ., Constr., and Env. Engrg., Oregon State University, Corvallis, OR 97331-2302, hallerm@engr.orst.edu

[2]Ocean and Terrestrial Applications, Veridian Systems Division, Ann Arbor, MI 48109

ing waves is the most well established remote sensing technique (Monahan 1971, Lippmann and Holman 1991; and many others).

While most studies of radar backscatter have taken place in deep water, recently there has been increased interest in using microwave radar as a tool for studying the nearshore environment. The few published applications of radar in the nearshore have suggested that radar measurements can be used to infer information on bottom frictional dissipation (Hwang et al. 1998), bathymetry (Bell 1999), and wave energy fluxes (McGregor et al. 1998). An interesting feature often found in radar returns from the open ocean is the presence of short-duration, large amplitude bursts of backscattered power. It has long been known that these spiky fluctuations (termed "sea spikes") are associated with steep and/or breaking waves (e.g. Katzin 1957, Long 1974). However, comparisons of simultaneous video and radar measurements have shown that sea spikes in the open ocean are not always caused by breaking wave events (Jessup et al. 1991, Liu et al. 1998, Frasier et al. 1998) and the exact relationship between wave characteristics and sea spikes remains unclear.

The following experimental study presents field measurements of microwave backscatter and simultaneous video from surf zone waves. This type of data is rare in the literature, and this study offers a unique opportunity to assess the backscattered field from shallow water breaking waves and to relate the measured radar quantities to the physical properties of the water waves.

EXPERIMENT DESCRIPTION

These experimental data were collected as a small addition to the multi-institutional SHOWEX experiment conducted at the U.S. Army Corps of Engineers Field Research Facility (FRF) in Duck, NC in the fall of 1999. The microwave backscatter measurements were made with a coherent, continuous-wave, polarized scatterometer operating at X-band (10.5 GHz) and vertical transmit and receive polarization.

The scatterometer was mounted alternately at two locations, first aboard the mobile CRAB and subsequently on the FRF pier. The data from the pier provided the most information regarding shallow water breaking waves, and this data is analyzed herein. During the collections a bore-sighted video camera was mounted on the scatterometer to record the optical signatures of breaking wave events. The 3-dB illuminated area of the radar was approximately 1.2 m $\times$ 1.6 m, which is small compared to the wavelength of the surf zone waves and the turbulent breaking regions filled a considerable fraction of the 3-dB footprint.

The grazing angles and look directions along with the number of data records for each run are listed in Table 1. Each record was approximately five minutes in duration. Measurements of the wind-wave directional spectrum and the ambient wind speed and direction are acquired nearly continuously by the FRF. The incident wave field on the day of the experiment was dominated by narrow-banded swell (H_{mo}=0.68 m, f_p=0.09 Hz) arriving from the east (90 deg. T). The winds were light at 3.9 m/s and from the southwest (206 deg. T).

TABLE 1. Viewing parameters for pier collection.

graz. ang. (deg.)	look dir. (deg. T)	radar records	video records
31	104	2	0
31	124	5	5
41	104	1	1
46	124	1	1
46	134	1	1
46	144	1	1

At 45° grazing the illuminated area was closer to the pier. Close to the pier, the local depression (under the pier) along with wave reflections from the pier pilings tend to complicate the wave field. This led to significant differences in the illuminated wave field between 30° and 45° grazing. In this short work we will concentrate on the less complicated wave field illuminated at 30°.

BREAKING WAVE DETECTION

The association of wave breaking with sea spikes has been known for several decades, however, relatively few quantitative comparisons between radar backscatter and optical signatures of wave breaking have been made. Lewis and Olin (1980) appear to be the first to make this comparison, and their study is also the only one to consider shallow water breaking waves. The most comprehensive comparison was made by Liu et al. (1998) who found that at low grazing angles (LGA) only approximately 30% of the the observed sea spike events were associated with deep water whitecaps, while the remainder were attributed to "steep" wave features. However, whitecaps accounted for a large percentage of the total backscattered power. In a related work, Frasier et al. (1998) found that a large range of whitecap coverages mapped to a comparably smaller range of sea spike coverages. Thus, they concluded that sea spike coverage has a significant dependence on ocean surface features that do not yield an optical signature.

Although sea spikes are more prominent in LGA measurements, they have been observed at all grazing angles (Lee et al. 1995). In addition, sea spikes observed at moderate grazing angles are better correlated with active wave breaking. Jessup et al. (1991) found that 70% of the sea spikes they observed, using a radar operating at K_u band and 45° grazing, were associated with whitecaps recorded by a bore-sighted video camera. Obviously, any technique for measuring wave breaking is dependent to some extent on the definition of what constitutes a wave breaking signature, whether its based on video intensity, backscattered power, or any other measurable quantity. Jessup et al. (1991) found the best correspondence between the microwave and optical breaking signatures occurred when the sea spikes were defined by a combination of Doppler bandwidth exceeding 50 Hz and normalized radar cross section (NRCS) values over -6 dB. But it should be noted that none of these previous studies have analyzed the measured optical

intensity signal, instead wave breaking was in the "eye of the beholder". Here we will perform a quantitative comparison between the microwave parameters and the measured intensity variations recorded by the video camera and show that there is a significant correlation between backscattered power and the size of the turbulent breaking region in shallow water breakers.

Radar sea spikes

In order to analyze the relationship between sea spikes at moderate grazing angles and shallow water breaking waves, a sea spike definition must be adopted. Here we define a sea spike as simply any excursion above the mean NRCS that contains more than one data point (sampling interval = 0.2 sec). This definition is chosen instead of the absolute NRCS threshold (-6 dB) of Jessup et al. (1991) for several reasons. First, their definition was based on measurements from only one grazing angle and it is presently unknown how the NRCS from active breaking regions depends on grazing angle. Secondly, an absolute power threshold is subject to calibration uncertainties between radar systems. Thirdly, the previous criteria were developed for wave breaking in the open sea, which is very different from shallow water breaking induced by interaction with the sea bottom. So the present definition is chosen for its simplicity.

Lewis and Olin (1980) were the first to consider the scattering from the highly roughened surface of whitecaps as a separate entity from the typical Bragg contribution. They hypothesized that whitecaps are isotropic radiators and therefore the NRCS of the breaking region should be approximately 3 dB. Following that line of reasoning, here we consider the NRCS time series as a summation of contributions from the sea spikes and the ambient background given by the following:

$$\sigma^0(t) = \sigma^0_{ss}(t) + \sigma^0_a(t) \tag{1}$$

where

$$\sigma^0_{ss} = \begin{cases} 0 & \sigma^0 < \overline{\sigma^0} \\ \sigma^0(t) & \sigma^0 > \overline{\sigma^0} \end{cases} \tag{2}$$

$$\sigma^0_a = \begin{cases} \sigma^0(t) & \sigma^0 < \overline{\sigma^0} \\ 0 & \sigma^0 > \overline{\sigma^0}. \end{cases} \tag{3}$$

The mean NRCS ($\overline{\sigma^0}$) for an individual record is

$$\overline{\sigma^0} = \frac{1}{T}\int_0^T \sigma^0(t)dt, \tag{4}$$

where T is the record duration ($T \approx 300$ sec for these data).

Figure 1 shows time series of NRCS collected at 31° grazing along with the mean NRCS used as the threshold for defining sea spikes. Frequent sea spikes are clearly evident and distinct from the low level ambient background signal. There were a total of 50 minutes of simultaneous video and radar measurements, which encompassed a range of grazing angles and look directions. An initial

comparison between the video records and the NRCS time series showed that for the 306 sea spikes observed in the radar data, 92% were associated with some degree of visual wave breaking. There was no restriction placed on the observed size of the breaking event, but only events that clearly occurred within the 3dB footprint were counted. A small number of incipient breakers or highly steepened unbroken waves also occurred during the observation period, yet, for these data the comparison with video indicates that the sea spike detector does a good job of sorting out the steep waves from the breaking waves. Thus, the comparison of the radar measurements with the video suggests that the measured sea spikes serve as a good detector of shallow water breaking events.

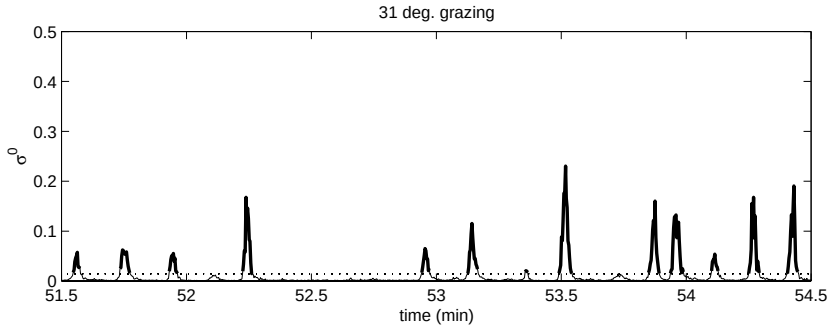

Fig. 1. Time series of NRCS measured at 31° grazing, excursions above threshold (sea spikes) are shown as thick lines.

Analysis of the set of individual spike maxima for each record indicated that there is some dependence of sea spike amplitude on grazing angle. However, there is no systematic dependence on look direction with respect to the waves for the range of angles considered here. In contrast, the ambient signal showed a significant increase with grazing angle, which is expected based on traditional models of two-scale Bragg scattering from non-breaking waves. Nonetheless, for moderate grazing angles these data suggest that surf zone sea spikes are clearly visible ($\sim$ 10-12 dB higher) above the ambient background.

Radar/Video comparison

The bore-sighted video camera was operated simulataneously with the radar and recorded black and white movies of the sea surface. The radar and video recordings were synchronized at the beginning of the pier collection using a time code generator. During post-processing, the movies were downsampled to a rate of 5Hz and digitized using Winnov Videum Capture image processing software on a standard PC. This allowed us to make quantitative comparisons between the gray scale intensity of the video images and the measured radar backscatter.

Figure 2 shows three video frames taken at 31° grazing. The superimposed circles near the centers of the images mark the perimeter of the 3dB radar footprint. The parallel transects are approximately oriented in the direction of wave propagation and traverse the wave profile at two different stages in the breaking process. The pixel intensities along the transects are shown in the right hand

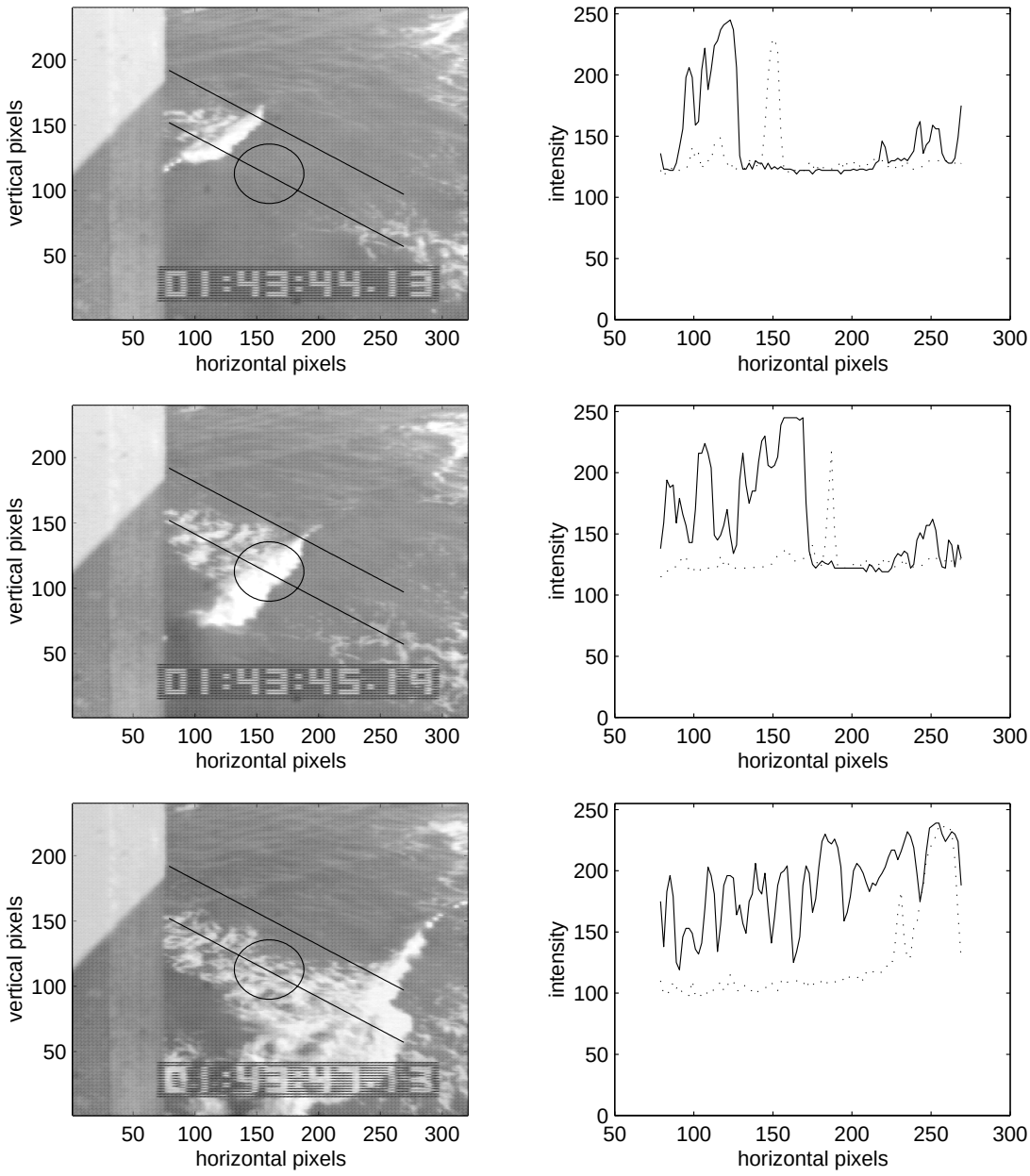

Fig. 2. (*left panels*) **Video frames obtained at 31° grazing** (*right panels*) **pixel intensities for the linear transects shown in video frames, lower transect (solid) upper transect (dotted). Gray scale intensity varies between 0 (black) and 255 (white).**

panels. In all three images the leading edge of the breaking region is well defined as a sharp increase in intensity in the upwave direction. The upper transects in each image cross the wave profile at earlier stages in the breaking process. For these transects the active breaking region appears as a well defined spike above a nearly constant darker background. As the wave propagates through the scene, the intensity spike widens and begins to develop another spike on its

trailing edge. These trailing high intensity regions are the result of relict turbulence and/or foam being shed from the wave crest and left behind. The lower transects cross the wave at later stages of breaking and show numerous trailing spiky features of gradually weakening intensity. This trailing foam is visible as a splotchy area in the video frame and often remains stationary on the water surface for many seconds before dissipating.

The results discussed earlier suggested that the radar sea spikes are well correlated with optical (whitewater) signatures of breaking waves and also that the radar backscatter from the active breaking regions is much greater than from other parts of the water surface. If, as suggested by Lewis and Olin (1980), the active breaking area can be considered an isotropic radiator then the instantaneous NRCS measured during a sea spike event should be correlated with the size of the illuminated breaking region. Assuming the dominant signal is from the breaking region, the NRCS during a sea spike event can be approximated by the following:

$$\sigma^0_{ss}(\alpha, t) \approx \frac{\sigma_b(\alpha, t)}{A_\alpha}, \tag{5}$$

where σ_b is the total radar cross section of the illuminated breaking region at grazing angle α, and A_α is the area of the 3dB footprint. The instantaneous cross section of the illuminated breaking area can be represented by

$$\sigma_b(\alpha, t) = \int_0^{A_b} \sigma^0_b(\alpha)\, G'(\theta, \phi)\, dA, \tag{6}$$

where A_b is the area of the breaking region within the footprint, σ^0_b is the NRCS within the breaking region (i.e. σ_b/A_b) and is assumed to be spatially constant but may be dependent on grazing angle, and G' is the antenna gain factor normalized such that $\int_0^{A_\alpha} G'\, dA = A_\alpha$. For a given grazing angle we can define a breaking area factor

$$I(t) = \frac{\int_0^{A_b} G' dA}{A_\alpha}, \tag{7}$$

which is the breaking area within the footprint weighted by the antenna gain pattern and varies between 0 (no breaking) and 1 (breaking area fills the footprint). Substituting Eq. 6 and Eq. 7 into Eq. 5 we obtain the following

$$\sigma^0_b(\alpha) = \frac{\sigma^0_{ss}(\alpha, t)}{I_{ss}(\alpha, t)}, \tag{8}$$

where I_{ss} is the breaking area factor during the sea spike events. Therefore, the NRCS of the active breaking region can be estimated from the measured NRCS if the breaking area factor can be appropriately estimated from the video.

Defining wave breaking and, therefore, estimating A_b in the video images can be difficult. For example, as seen in Figure 2, while an absolute intensity threshold may be applied to the upper transects to define the breaking region, a similar threshold applied to the lower transect is likely to include relict foam

in the breaking region. In addition, it is unclear how comparisons can be made between different viewing geometries, since pixel intensity is a relative measure dependent on the ambient light conditions and the camera aperture. However, at this stage imposing an intensity threshold seems to be the simplest first approach. Therefore we impose a threshold intensity value whereby the brightest regions of the image are isolated and defined as active breaking regions. The procedure is to scan the 3dB footprint in each video frame for intensity values exceeding the threshold and then create a binary mask of ones and zeros where the ones are the locations of pixels exceeding the threshold (we do not require the mask to be continuous). This mask demarcates A_b and is then applied to the antenna gain pattern, G', and the breaking area factor time series can be calculated from Eq.7.

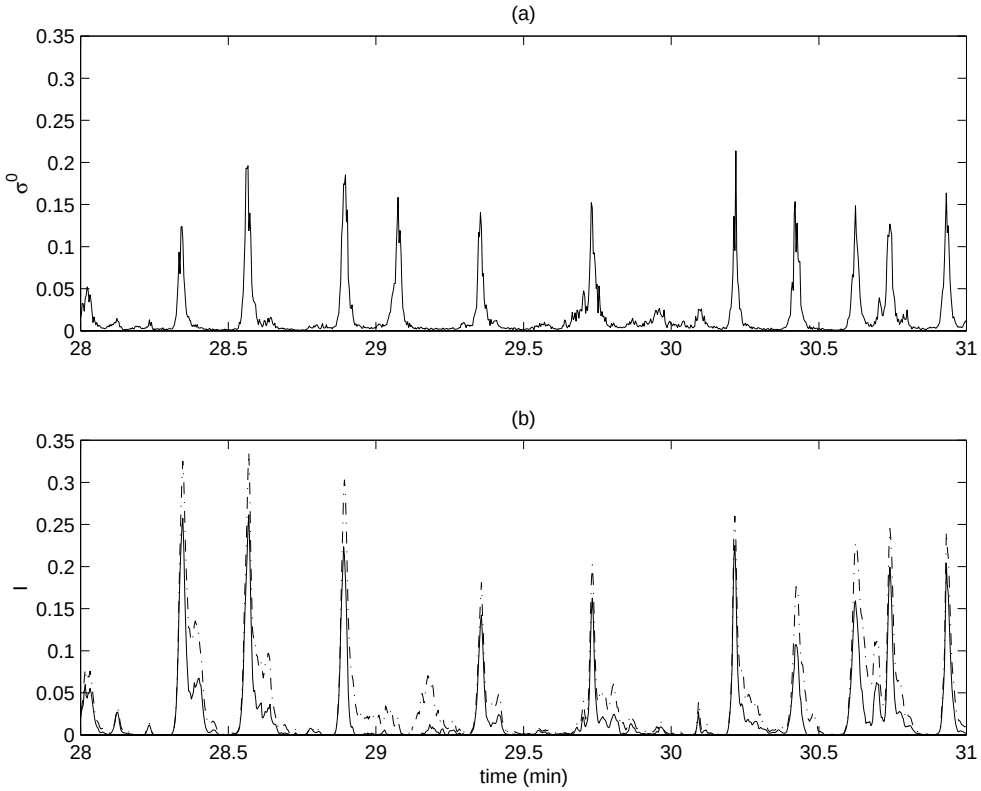

Fig. 3. (a) σ^0 **at 31° grazing** (b) **corresponding breaking area factor using a gray scale intensity threshold of 215 (solid) and 205 (dash-dot).**

Figure 3 shows time series of σ^0 and I. It is evident that for both intensity thresholds used the breaking area factor shows numerous spiky fluctuations similar to σ^0. Although both time series appear to be very well correlated, there are some differences. For example, just after t =29 minutes there is a sea spike that does not have a corresponding area spike. Examination of the video shows that this sea spike occurrs simultaneously with a breaking wave, but this wave had been breaking for several meters before it entered the footprint. As the breaking proceeded the whitewater became well mixed and splotchy. Therefore, the

video image of the breaking region passed below the intensity threshold and did not generate an area spike. Nonetheless, the increased surface roughness of the breaker generated a sea spike. This type of mismatch between the sea spikes and the area spikes was not common, but it does point out that the two sensors are measuring somewhat different quantities. However, the radar backscatter appears to be especially tuned to the turbulent breaking region very near the wave crest. In fact, the three video frames shown in Figure 2 correspond to the initiation of the sea spike (i.e. σ^0 rises above $\overline{\sigma^0}$), the sea spike maximum, and the conclusion of the sea spike event. In other words, the sea spike is initiated as the breaking wave enters the 3dB footprint, reaches its maximum amplitude when the breaker is at bore center, and ceases a short time after the crest has exited the footprint.

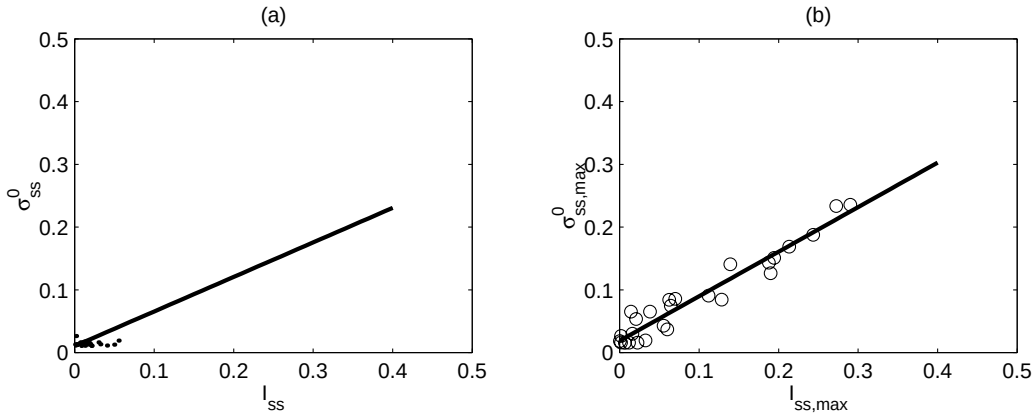

Fig. 4. Instantaneous σ^0_{ss} vs. I_{ss} (a) during sea spike events (slope=0.55, r^2=0.88) and (b) only at sea spike maxima (slope=0.71, r^2=0.97).

Figure 4a directly compares the instantaneous values of σ^0_{ss} and I_{ss} (using a threshold of 225) during all the sea spike events from the same data record that generated Figure 2. The data strongly suggest a linear relationship between the measured NRCS and the breaking area factor calculated from the video. A linear fit to the data was calculated using a least squares method and the NRCS of the breaking region is given by the slope of this line (σ^0_b=-2.6 dB, see Eq. 8). In order to eliminate some of the scatter due to the relict foam in the video images, only the instantaneous values at the sea spike maxima are shown in Figure 4b. The NRCS maxima are highly correlated (r^2=0.97) with their simultaneous breaking area factors. The linear fit using only the sea spike maxima suggests σ^0_b=0.71 (-1.5 dB).

CONCLUSIONS

Simultaneous microwave radar and video camera signals generated by shallow water breaking waves at a field beach are presented. The backscattered power measured by the radar was compared to video estimates of the size of the breaking region within the radar footprint. The backscattered power was shown to be well correlated with the area of the breaking region. Based on an analysis of

a number of data records (only one record was presented herein due to space limitations), the RCS per unit area of the turbulent breaking region appears to be well approximated by a constant value of -2 dB ($\pm$ 0.5 dB).

These results indicate that microwave radar is a good breaking wave detector and can be used for the measurement of the spatial and temporal variations of wave breaking. In addition, X-band radar offers the dual advantages of not being sensitive to the ambient light conditions and is also less sensitive to the relict foam generated in the breaking process that is not related to active wave breaking.

ACKNOWLEDGMENTS

The authors would like to thank the staff of the FRF for their considerable help during the field experiment and also Zandy Williams of Arete Associates for providing the video equipment.

REFERENCES

Bell, P.S., 1999. Shallow water bathymetry derived from an analysis of X-band marine radar images of waves. *Coast. Eng., 37*, 513-527.

Ding, L. and Farmer, D.M., 1994. Observations of breaking surface wave statistics. *J. Phys. Oceanogr.*, **24**, 1368-1387.

Frasier, S.J., Liu, Y., and McIntosh, R.E., 1998. Space-time properties of radar sea spikes and their relation to wind and wave conditions. *J. Geophys. Res., 103*, 18,745-18,757.

Gemmrich, J.R. and Farmer, D.M., 1999. Observations of the scale and occurrence of breaking surface waves. *J. Phys. Oceanogr.*, **29**, 2595-2606.

Hwang, P.A., Walsh, E.J., Krabill, W.B., Swift, R.N., Manizade, S.S., Scott, J.F., and Earle, M.D., 1998. Airborne remote sensing applications to coastal wave research. *J. Geophys. Res., 103*, 18,791-18,800.

Jessup, A.T., Melville, W.K., and Keller, W.C., 1991. Breaking waves affecting microwave backscatter 1, Detection and verification. *J. Geophys. Res., 96*, 20,547-20,559.

Jessup, A.T., Zappa, C.J., Loewen, M.R., and Hesany, V., 1997. Infrared remote sensing of breaking waves. *Nature*, **385**, 52-55.

Katzin, M., 1957. On the mechanism of radar sea clutter. *Proc. IRE, 45*, 44-54.

Lee, P.H.Y., Barter, J.D., Beach, K.L., Hindman, C.L., Lake, B.M., Rungaldier, H., Shelton, J.C., Williams, A.B., Yee, R., and Yuen, H.C., 1995. X band microwave backscattering from ocean waves. *J. Geophys. Res., 100*, 2,591-2,611.

Lewis, B.L. and Olin, I.D., 1980. Experimental study and theoretical model of high-resolution radar backscatter from the sea. *Radio Sci., 15*, 815-828.

Lippmann, T.C. and Holman, R.A., 1989. Quantification of sand bar morphology: A video technique based on wave dissipation. *J. Geophys. Res., 94*, 995-1011.

Lippmann, T.C. and Holman, R.A., 1991. Phase speed and angle of breaking waves measured with video techniques. *Proc. of Coastal Sediments '91*, 542-556.

Liu, Y., Frasier, S.J., and McIntosh, R.E., 1998. Measurement and classification of low-grazing-angle radar sea spikes. *IEEE Trans. on Antennas Propag., 46.*

Long, M.W., 1974. On the two-scatterer theory of sea echo. *IEEE Trans. Antennas Propag., AP-22*, 667-672.

McGregor, J.A., Poulter, E.M. and Smith, M.J., 1998. S band Doppler radar measurements of bathymetry, wave energy fluxes, and dissipation across an offshore bar. *J. Geophys. Res., 103*, 18,779-18,789.

Monahan, E.C., 1971. Oceanic whitecaps. *J. Phys. Oceanogr.*, **1**, 139-144.